J Mater Sci (2009) 44:4840–4847
DOI 10.1007/s10853-009-3738-7

μ-Phase behavior in a cast Ni-base superalloy

X. Z. Qin · J. T. Guo · C. Yuan · G. X. Yang · L. Z. Zhou · H. Q. Ye

Received: 28 February 2009 / Accepted: 9 July 2009 / Published online: 23 July 2009

Abstract The response of μ phase to applied stress and long-term thermal exposure has been investigated in the cast Ni-base superalloy K446. It is found that during stress rupture, the applied stress accelerates the precipitation and growth of μ phase. However, during thermal exposure the μ phase precipitating in the form of needles and granules experiences a complicated evolution. The needles, fiber- or sheet-shaped in three-dimension, align very regularly during exposure, either lying in three directions with an acute angle to one another or in two directions perpendicular to each other, the mechanisms of which are characterized in detail. In addition, it is concluded that an excessive precipitation of μ phase severely degrades the mechanical properties of the alloy, whereas its evolution behavior during thermal exposure is determined to have an insignificant influence on the properties.

Introduction

K446 alloy is a newly developed cast Ni-base superalloy, designed for microstructural component applications of gas turbines, which has good mechanical properties, oxidation resistance, and hot-corrosion resistance under laboratory conditions. However, this alloy contains a large amount of refractory elements, such as W and Mo, rendering it prone to the precipitation of topologically close-packed (TCP) phases during thermal exposure at elevated temperature.

X. Z. Qin (✉) · J. T. Guo · C. Yuan · L. Z. Zhou · H. Q. Ye
Institute of Metal Research, Chinese Academy of Sciences, Shenyang 110016, China
e-mail: xzqin@imr.ac.cn

G. X. Yang
Dongfang Turbine Co., Ltd, Deyang 618201, China

Topologically close-packed phases are paid great attention because of their important influence on the properties of superalloys. It is generally accepted that precipitation of TCP phases depletes the strengthening elements from the γ matrix and accordingly softens the alloys [1–4]. Nevertheless, some controversies are also significant on these intermetallic phases. For example, Acharya and Fuchs [5] thought that stress decreased the amount of σ phase in CMSX-10 alloy, while Reed et al. [6] insisted that the presence of a tensile stress accelerated the σ precipitation in UDIMET 720 alloy. In addition, some researchers reported that the voids initiated at brittle TCP phases could act as the initiation sites for fracture [7–9], whereas others considered that these voids did not actually contribute to the fracture [2, 4, 10]. Even recently, some investigators [11] have alleged that the TCP μ phase in K465 alloy could produce large plastic deformation, which is completely opposite to the traditional viewpoint of brittleness.

TCP phases such as σ and μ are the common constituent phases of modern superalloys, which often occur during extended service or thermal exposure. Therefore, to further improve the properties of superalloys, it is undoubtedly important to eliminate the disagreements mentioned above. In this article, not only the effects of tensile stress on the precipitation of μ phase are examined, but also the precipitation and evolution of μ phase during long-term thermal exposure and their influence on the mechanical properties of K446 alloy are evaluated.

Experimental

The composition of K446 alloy is given in Table 1. The specimens used in the present investigation were subjected

Table 1 Composition of K446 alloy

	C	Cr	Al	Ti	Nb	Mo	W	Fe	Ni
wt%	0.1	16	1.8	2.4	1.1	3.5	5	15	Balance
at.%	0.5	18	3.9	3	0.7	2.1	1.6	15.8	Balance

to a homogenization for 4.5 h at 1110 °C (air cooling) and then an annealing treatment was carried out for 10.5 h at 750 °C (air cooling).

After heat treatment, the specimens were divided into two groups, one for stress-rupture tests (Group A) and the other for long-term thermal exposure treatments (Group B). The Group A specimens were machined into cylindrical, threaded creep test bars (gauge diameter 7 mm, gauge length 26 mm), which were stress ruptured at 800 °C with the stress of 294 MPa (the lifetime was computed to be about 750 h). The Group B specimens were given a long-term, unstressed thermal exposure at temperatures of 800, 850, and 900 °C, respectively: the exposure times at 800 °C were designed to be 1000, 3000, 5000, and up to 10000 h, whereas the times at 850 and 900 °C only included 1000, 3000, and 10000 h. Then, tensile- and stress-rupture tests were performed under the conditions of 800 and 800 °C/294 MPa, respectively.

The microstructures were examined using optical microscopy (OM) and scanning electron microscopy (SEM). Chemical etching was employed for general microstructural observation, using a solution containing 20-g $CuSO_4$, 50-mL HCl, and 100-mL H_2O, which dissolves γ'. Deep etching with an electrolyte of 10-pct HCl in methanol, which removes both the γ and the γ', was utilized for the three-dimensional observation of μ phase. The specimens functioned as the

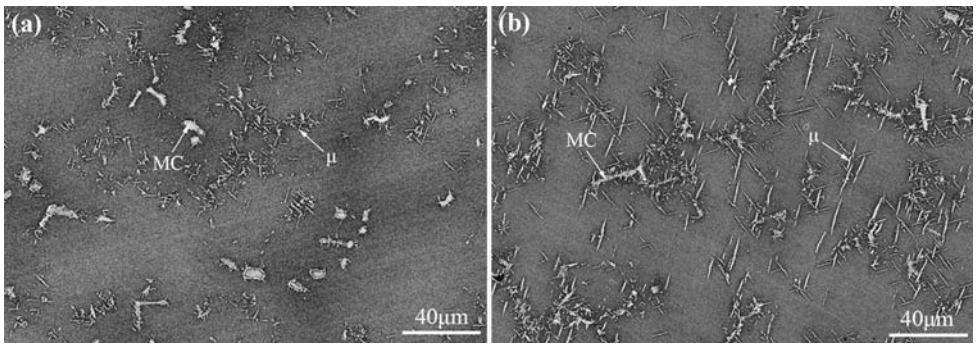

Fig. 1 Distribution features of μ phase in the threaded region (**a**) and gauge section (**b**) of the stress-ruptured bars

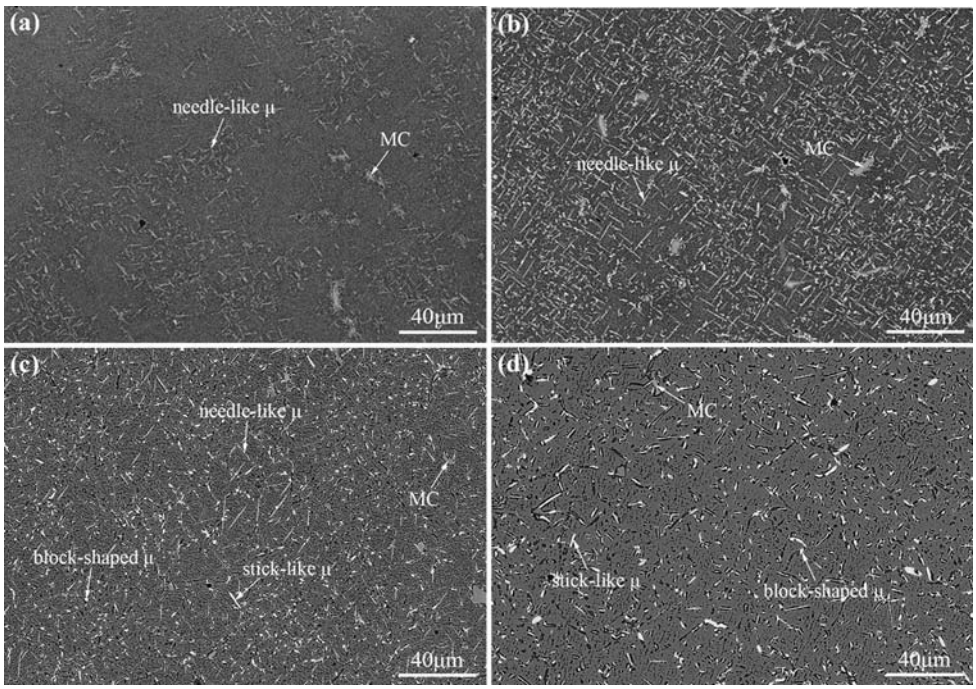

Fig. 2 Precipitation and evolution of μ phase within the grains with increased exposure temperature or time
a 800 °C/1000 h,
b 850 °C/3000 h,
c 850 °C/10000 h,
d 900 °C/10000 h

anode, while the cathode was a stainless steel plate; the current density was ~ 0.5 A/cm^2.

Transmission electron microscopy (TEM) equipped with an energy dispersive X-ray spectroscope (EDS) was employed mainly for phase identification. Foils for TEM were prepared on a twin-jet electropolisher with a solution of 10% perchloric acid and 90% ethanol.

Results and discussion

The microstructure of heat-treated K446 alloy consists of γ matrix, γ' precipitate, primary MC carbide, and grain boundary $M_{23}C_6$ and M_6C carbides. When the alloy is held at high temperatures for a long time, e.g., during stress-rupture tests or long-term thermal exposure, the μ phase precipitates heavily from the γ matrix, which depends on both the applied stress and the exposure parameters (temperature and time).

Effect of applied stress on the precipitation of μ phase

In the Group A bars, the cross-section area of the gauge section is much smaller than that of the threaded region; therefore, the gauge section will suffer from a larger stress than the threaded region when the bars are under the applied stress.

During stress rupture, the μ phase precipitates from the supersaturated γ matrix. In the failed bars, the size and distribution density of μ phase significantly change from place to place (Fig. 1): in the threaded region, the μ phase is small and sparse (Fig. 1a), whereas it is coarse and dense in the gauge section, whether near or far from the rupture site (Fig. 1b). Since the threaded region and the gauge section are under the same conditions except the stress, it can be concluded that the stress plays a decisive role in the distribution difference of μ phase at the different locations, or more exactly, that the stress in fact accelerates the precipitation and growth of μ phase in the gauge section, where the stress is greater relative to the threaded region. This conclusion is in disagreement with Pessah et al's [4] report, where they claim that stress slowed down the precipitation of μ phase in the MC2 alloy.

Primary MC carbide absorbs a significant amount of refractory elements such as W and Mo from the ambient matrix during solidification, but it cannot easily release these elements into the alloy bulk [12]; therefore, in the threaded region, the μ phase precipitates far from the carbide due to the depletion of the elements (Fig. 1a). However, in the gauge section, the applied stress reinforces the diffusion of elements [6] and accordingly induces the μ phase to form throughout the interdendritic regions, including around the primary carbide (Fig. 1b).

μ-Phase evolution during long-term thermal exposure

Precipitation and evolution of μ phase

It is generally accepted that Mo partitions to the interdendritic regions during solidification in common cast

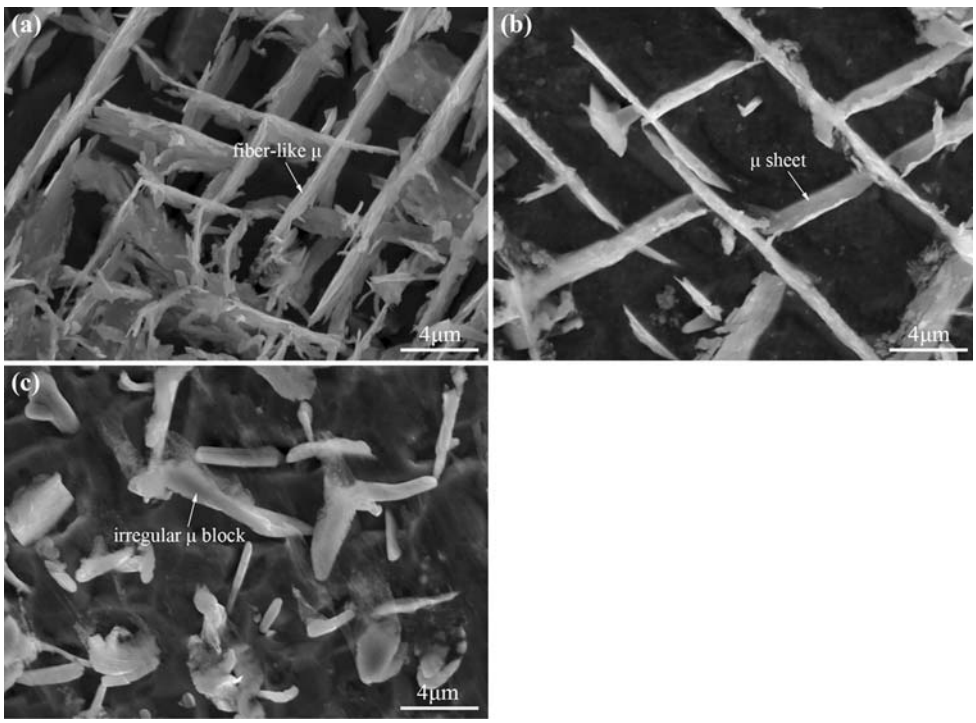

Fig. 3 Three-dimensional observation of μ phase under the different exposure conditions
a 800 °C/1000 h,
b 850 °C/3000 h,
c 900 °C/10000 h

Ni-base superalloys [8, 13, 14] and compared with other refractory elements, has a stronger tendency to form the μ phase [14, 15]. Accordingly, in the present alloy with a high W + Mo content, the μ phase precipitates firstly at the interdendritic regions, and then in the W-enriched dendritic cores in the Group B specimens during thermal exposure [16, 17].

Within the grains, the μ phase precipitates in the form of needles and granules, and its amount, size, and morphology experience a notable evolution with extended exposure (Fig. 2). For the needles, their amount and size tend to present a peak value with increased exposure temperature or time, but they eventually disappear, probably transforming into the stick- or block-like μ, or dissolving into

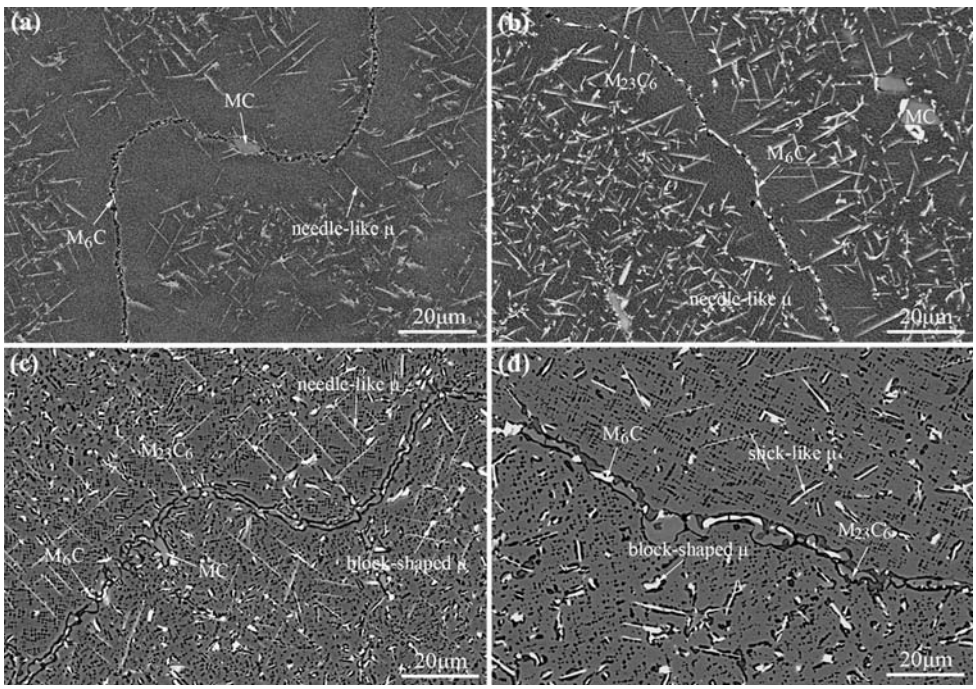

Fig. 4 Precipitation and evolution of μ phase near the grain boundaries with creased exposure temperature or time **a** 800 °C/1000 h, **b** 850 °C/3000 h, **c** 850 °C/10000 h, **d** 900 °C/10000 h

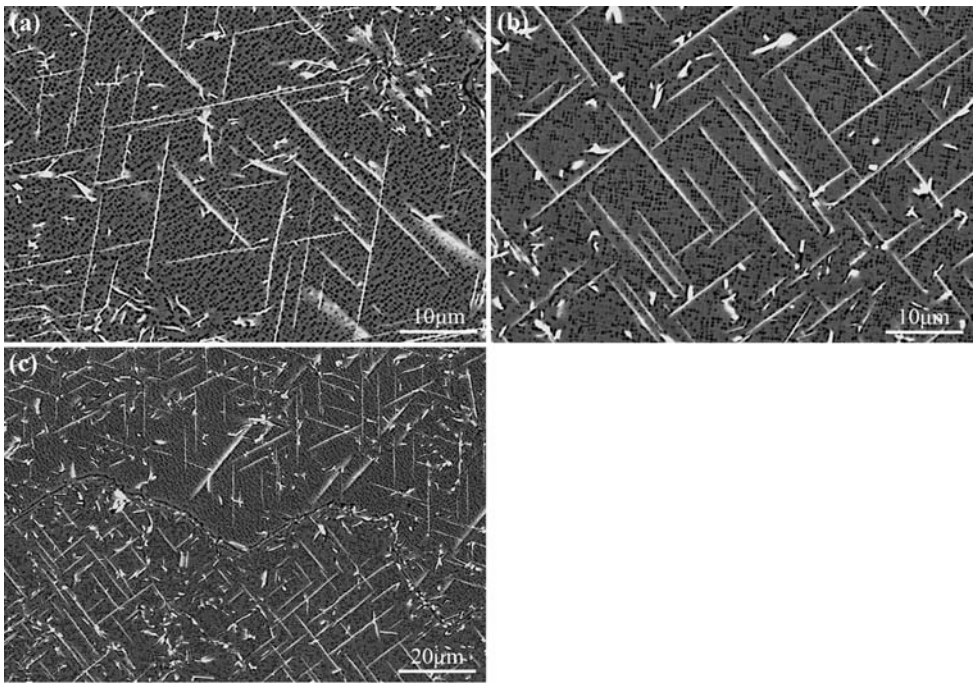

Fig. 5 Regular alignment of μ needles under the different exposure conditions **a** 800 °C/1000 h, **b** 850 °C/10000 h, **c** 850 °C/1000 h

the γ matrix at the condition of 900 °C/10000 h. In contrast, the granules continuously grow during the whole period of exposure and finally develop into the irregular blocks. It is unexpected that there are no M_6C carbides found in the evolution process, which is very different from the previous observation results [4, 15–18].

A deep etching technique was used to observe the three-dimensional appearance of μ phase, which clearly displayed the morphological transition of the needle-shaped μ from a fiber-like structure to coarse sheets to irregular blocks during thermal exposure (Fig. 3).

At the grain boundaries, the μ phase also undergoes a complex evolution, but it is a bit different from the evolution process present within the grains, as exhibited in Fig. 4. At the initiation of exposure, the μ phase is absent due to the shortage of refractory elements, such as Cr, W, and Mo, which have probably segregated to the boundaries and combined with C into M_6C and $M_{23}C_6$ carbides (Fig. 4a) [19, 20]. Then, as C is gradually exhausted with prolonged exposure, the μ precipitation is closer and closer to the boundaries owing to the re-enrichment of the elements (Fig. 4b, c). Finally, during the late exposure, most of the μ needles disappear, dissolving into the γ matrix or the boundaries, under the exposure condition of 900 °C/10000 h (Fig. 4d).

Alignment of μ needles and its mechanism

In this alloy, the μ needles arrange very regularly, either lying in three directions with an acute angle to one another (Fig. 5a) or in two directions perpendicular to each other (Fig. 5b); the former generally occurs more frequently than the latter. In Fig. 5c, the two styles of alignment are bounded by a grain boundary, suggesting that the alignment of μ needles is possibly different even in the adjacent grains.

The alignment of μ needles is closely related to the orientation relationship between the needles and the γ matrix, i.e., $\{0001\}_\mu // \{111\}_\gamma$ with $\langle 10\bar{1}0\rangle_\mu // \langle 110\rangle_\gamma$ (Fig. 6). When the needles, virtually sheet-shaped in three-dimension, nucleate in the matrix, their (0001) planes form a nice coherence relationship with one of the four {111} planes of the matrix; therefore, a regular μ tetrahedron whose surfaces superpose the {111} planes of the matrix is in effect build by the μ sheets, as sketched in Fig. 7a, where the cube in thin line represents a unit cell of γ matrix and the bold line tetrahedron in the cube characterizes the μ tetrahedron.

If the tetrahedron is cut along the (001) plane and is observed from the [001] direction, two groups of μ needles perpendicular to each other occur (Fig. 7b); whereas, if it is cut along the (110) or (111) plane and is seen from the [110] or [111] direction, three groups of needles are visible with an acute angle to one another (Fig. 7c, d). This is how

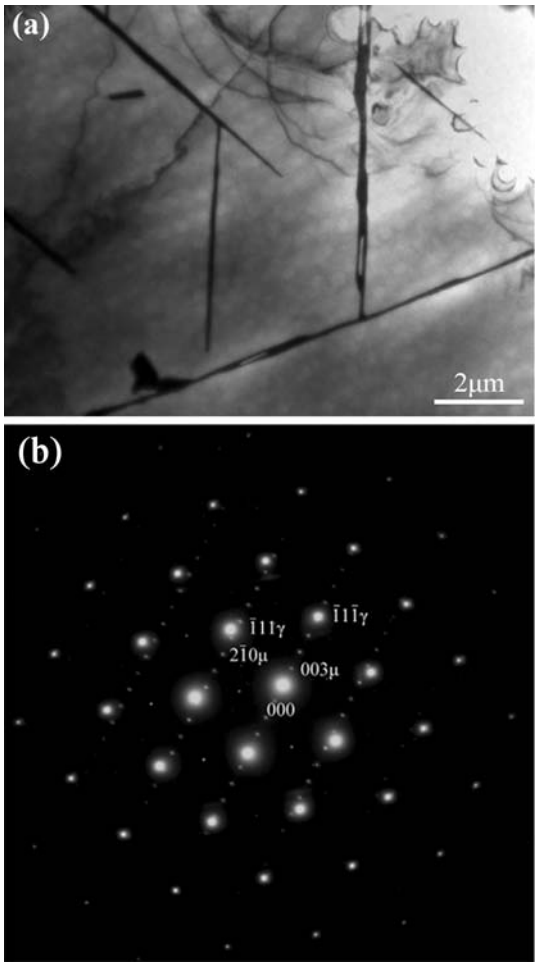

Fig. 6 TEM photograph of μ phase (**a**) and selected-area diffraction patterns of μ and γ (**b**) in the 850 °C/5000 h thermal-exposure specimen

and why the observed regular alignment patterns of μ needles occur in the present experiment.

Blocky-shaped μ phase

As described in "Precipitation and evolution of μ phase", the blocky-shaped μ phase can be developed from the μ granules, which precipitated from the supersaturated matrix at the early exposure stage. Faults are often found along the different crystal directions on the blocky-shaped phase (Fig. 8), which is thought to be associated with the intergrowth of tetrahedrally close-packed sheets with the ZrAl and MgCu type of structures [21, 22].

Also, during thermal exposure the acicular μ phase has a tendency to transform itself into the blocky-shaped μ, to minimize the interfacial energy. In Fig. 9a, several blocky-shaped nuclei are forming at the expense of the μ needle; and, in Fig. 9b, the interface between the needle and the block is clearly visible. These facts indicate that the

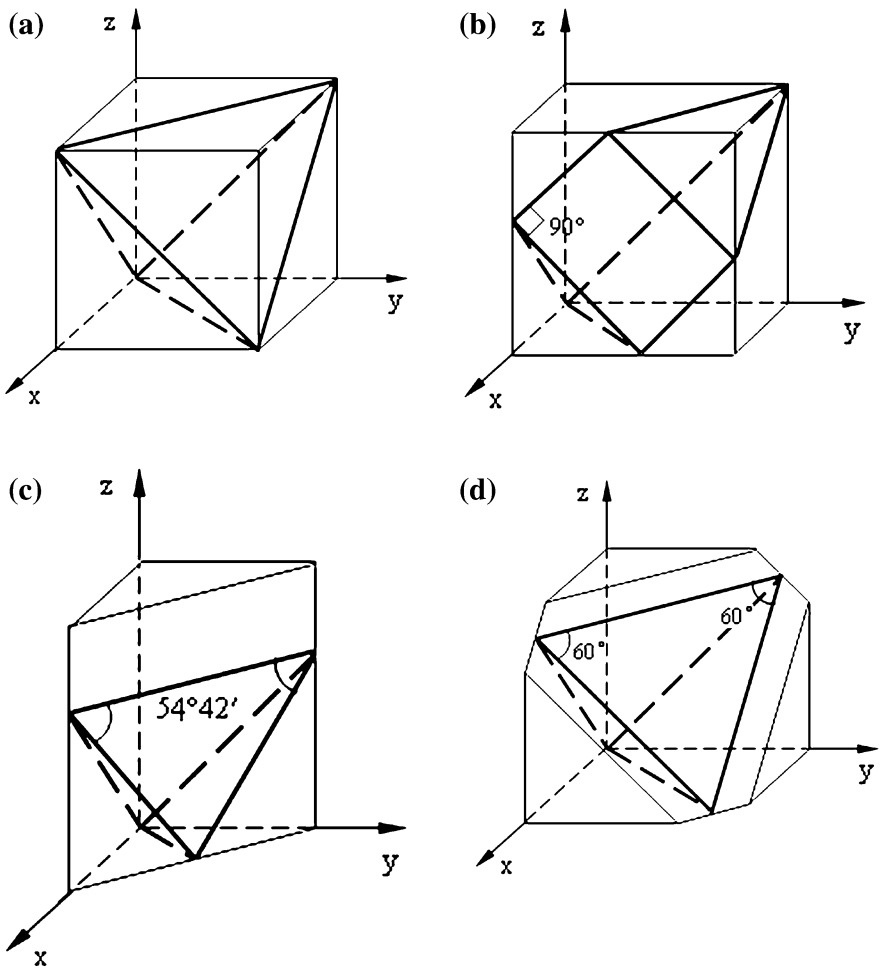

Fig. 7 Alignment mechanism of μ needles **a** the μ tetrahedron in the unit cell of the matrix; **b** the alignment pattern of μ needles along the (001) plane; **c** the alignment pattern of μ needles along the (110) plane; **d** the alignment pattern of μ needles along the (111) plane

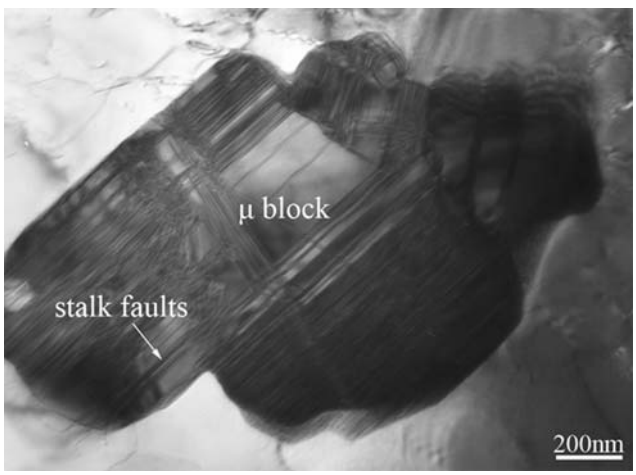

Fig. 8 TEM photograph of block-shaped μ phase precipitating from the γ matrix in the 800 °C/10000 h thermal-exposure specimen

morphological transition from acicular to blocky is probably an important reason for the disappearance of μ needles during the late stage of exposure (Fig. 2).

In Table 2, the acicular- and blocky-shaped μ have very similar chemical compositions. The atomic contents of Cr, Fe, Ni, and W + Mo in these two phases are all equivalent, respectively, even if the W/Mo ratio is larger in the acicular phase (1.58) than in the blocky phase (0.91). This suggests that the W/Mo ratio is likely the decisive factor which determines the μ phase in this alloy to exhibit the different morphologies, blocky and acicular, during thermal exposure.

Effect of μ phase on the rupture behaviors of specimens

The regular alignment of μ needles near the fracture site is severely destroyed during tensile- or stress-rupture tests (Fig. 10a), most of the needles tend to become parallel to the applied stress while a few tend to be perpendicular to the stress; the former is generally broken into many small segments, and no cracks are observed to occur between the segments [2, 4, 10]. However, cracks are occasionally

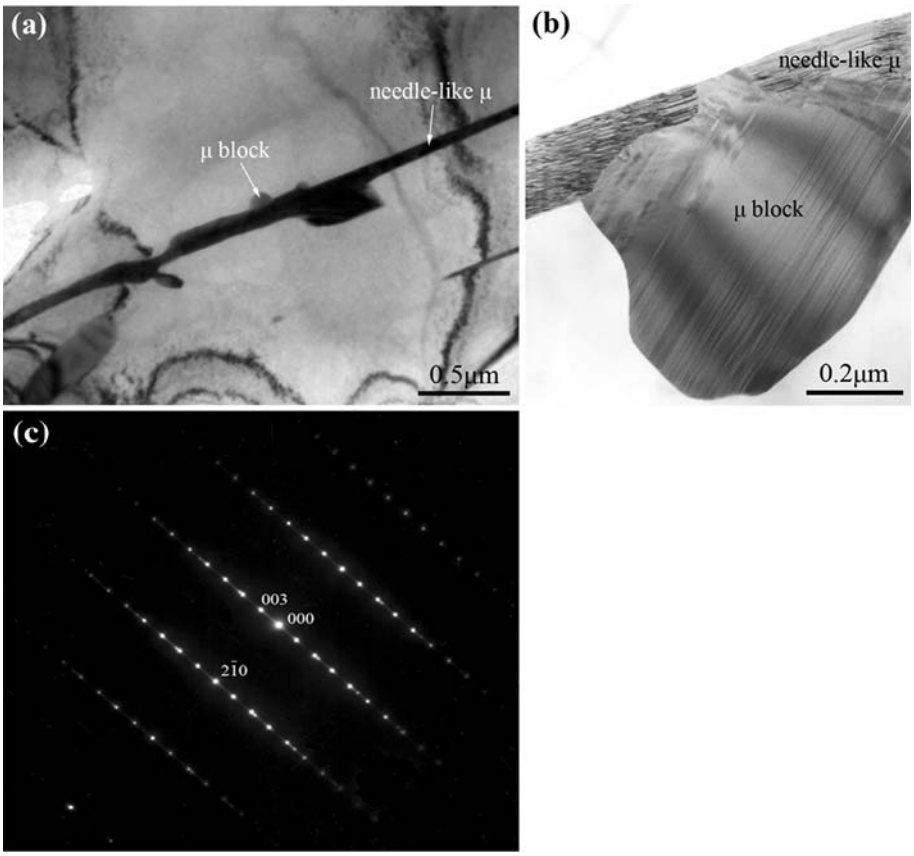

Fig. 9 TEM observations of block-shaped μ phase nucleating from the acicular μ phase **a** low-magnification photograph, 800 °C/5000 h; **b** high-magnification photograph, 900 °C/10000 h; **c** selected-area diffraction pattern of the block-shaped μ phase

Table 2 Chemical composition of acicular- and blocky-shaped μ (at.%)

	Cr	W	Mo	Fe	Ni
Acicular μ	21.5	24.9	15.8	16.3	21.5
Blocky μ	21.8	19.2	21	16.6	21.4

present on the periphery of the segments, the initiation of which can be attributed to the weak needle/needle cross connections, as illustrated in Fig. 10b.

In Fig. 11, some of μ needles normal to the applied stress have a bent appearance, which seem to indicate that the μ phase is a bit ductile in the present alloy. Nevertheless, careful observation reveals that the bent needles are always accompanied by microcracks as illustrated in the magnified photograph on the right. This is in agreement with the widely accepted viewpoint that μ phase is a fragile phase and has no beneficial effects on superalloys [9].

Apart from γ' coarsening, the precipitation of TCP μ phase during thermal exposure is a crucial factor which is responsible for the degradation of mechanical properties [1–4]. Accordingly, it is easily understood that the tensile strength and stress-rupture life of the alloy show a sharp drop in the period of 1000 h exposure when the μ phase fills the matrix (Table 3). The precipitation of μ phase heavily withdraws the efficient strengthening elements W and Mo from the γ matrix, resulting in an even more remarkable weakening effect on the matrix than the γ' coarsening that mainly depletes Al and Ti. However, it is evident that the evolution behavior of μ phase, which occur during thermal exposure, has an insignificant influence on the properties of the alloy.

Conclusions

(i) During stress rupture, the applied stress can accelerate the precipitation and growth of μ phase.

(ii) During thermal exposure, the μ phase precipitates in the form of needles and granules and experiences a complicated evolution. The needles lie either in three directions with an acute angle to one another or in two directions perpendicular to each other, the mechanisms of which are characterized in detail.

(iii) During tensile- or stress-rupture, microcracks occasionally occur around the segmented μ particles, the initiation of which is ascribed to the weak μ-needle/μ-needle cross connections.

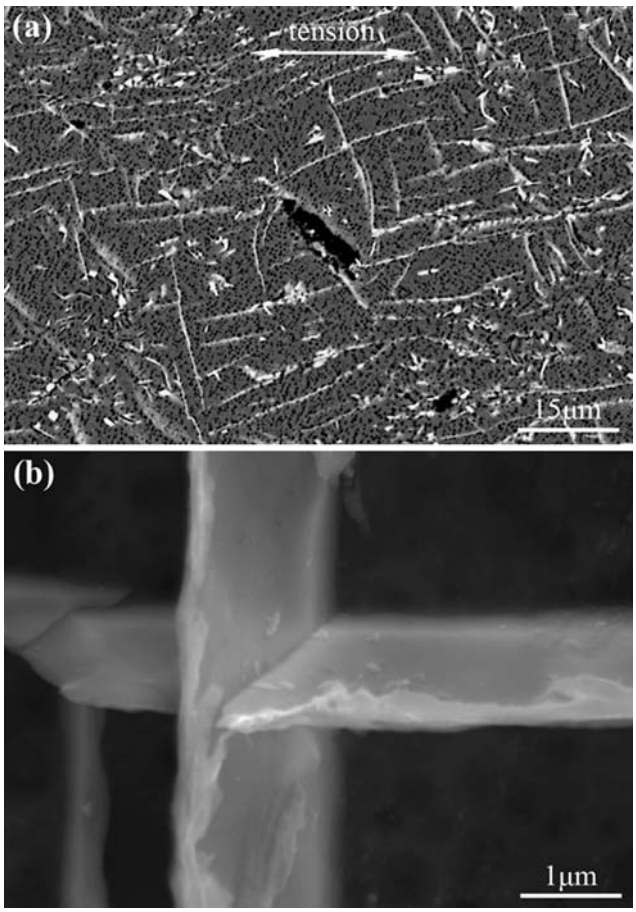

Fig. 10 SEM photographs of a crack near the μ segments in the specimen which was exposed at 800 °C/10000 h and then tensile ruptured at 800 °C (**a**) and two intersectional μ needles in the 850 °C/1000 h thermal-exposure specimen (**b**)

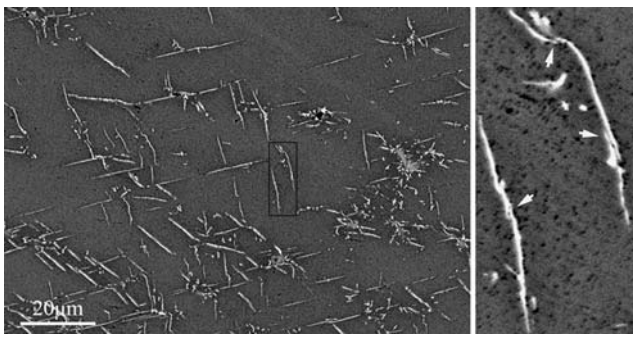

Fig. 11 Bended μ needles near the rupture site in a Group A specimen. On the *right* is the magnified photograph of the μ needles in the *black line rectangle*, in which the *arrows* point to the microcracks on the needles

(iv) The excessive precipitation of μ phase severely degrades the mechanical properties of the alloy, whereas its evolution during thermal exposure is determined to have an insignificant influence on the properties.

Table 3 The tensile- and stress-rupture data of specimens exposed at 850 °C with different times

Thermal exposure duration		0 h	1000 h	3000 h	10000 h
Tensile rupture (800 °C)	Yield strength/MPa	702	459.5	511.3	427.9
	Elongation/%	5.4	28.8	18.2	14.6
Stress rupture (800 °C/294 MPa)	Rupture life/h	750	77.5	32	20.3
	Elongation/%	12.2	20.8	28.3	24.9

Acknowledgement The authors would like to thank Prof. X. X. Jiang, Institute of Metal Research, Chinese Academy of Sciences, for her technical help in the deep etching.

References

1. Volek A, Singer RF, Buergel R, Grossmann J, Wang Y (2006) Metall Mater Trans A 37A:405
2. Simonetti M, Caron P (1998) Mater Sci Eng A 254:1
3. Khan T, Caron P, Duret C (1984) In: Gell M et al (eds) Superalloys. TMS, Warrendale
4. Pessah M, Caron P, Khan T (1992) In: Antolovich SD et al (eds) Superalloys. TMS, Warrendale
5. Acharya MV, Fuchs GE (2006) Scripta Mater 54:61
6. Reed RC, Jackson MP, Na YS (1999) Metall Mater Trans A 30A:521
7. Rae CMF, Karunaratne MSA, Small CJ, Broomfield RW, Jones CN (2000) In: Pollock TM et al (eds) Superalloys. TMS, Warrendale
8. Cai YL, Zheng YR (1982) Acta Metall Sin 18:30
9. Ross EW, Sims CT (1987) In: Sims CT et al (eds) Superalloys II. Wiley, New York
10. Chen QZ, Jones N, Knowles DM (2002) Acta Metall 50:1095
11. Yang JX, Zheng Q, Sun XF, Guan HR, Hu ZQ (2006) Scripta Mater 55:331
12. Qin XZ, Guo JT, Yuan C, Hou JS, Ye HQ (2008) Mater Lett 62:2275
13. Zupanič F, Bončina T, Križman A, Tichelaar FD (2001) J Alloy Compd 329:290
14. Zheng YR (1999) Acta Metall Sin 35:1242
15. Ma WY, Han YF, Li SS, Zheng YR, Gong SK (2006) Acta Metall Sin 42:1191
16. Zhao K, Ma YH, Lou LH, Hu ZQ (2005) Mater Trans 46:54
17. Yang JX, Zheng Q, Sun XF, Guan HR, Hu ZQ (2007) Mater Sci Eng A 465:100
18. Tawancy HM (1996) J Mater Sci 31:3929. doi:10.1007/BF00352653
19. Schulze C, Feller-Kniepmeier M (2001) Scripta Mater 44:731
20. Dumbill S, Boothby RM, Williams TM (1991) Mater Sci Tech 7:385
21. Andersson S (1978) J Sol St Chem 23:191
22. Carvalho PA, Hosson JTMD (2001) Scripta Mater 45:333